



# Study of Activation Energy of Magnetohydrodynamic Radiative Casson Nanofluid With Heat Source/sink and Cattaneo Christov Heat Flux Model Over Exponential Stretching Sheet

Mohammed Younus<sup>\*1</sup> and A. Venkatalakshmi<sup>2</sup>

<sup>1</sup> Department of Mathematics, Keshav Memorial Institute of Technology, Hyderabad, Telangana, India

<sup>2</sup> Department of Mathematics, University College of Science, Osmania University, Hyderabad, Telangana, India

\*Corresponding author: younus@kmit.in

Received: February 9, 2024

Accepted: April 22, 2024

**Abstract.** The present work uses numerical analysis to examine the *activation energy* (A.E.) of a *magnetohydrodynamic* (MHD), mixed convective, radiative Casson nanofluid with heat source/sink, Cattaneo Christov's heat flow model, "zero normal flux of the nanoparticles" across an exponentially stretched sheet, together with convective boundary condition. Numerous parameters' impacts on the temperature profile, velocity, and concentration profile were graphically interpreted after investigation. The findings are very comparable to those found in openly available literature. The velocity profile was observed for Casson fluid parameter ( $\beta$ ) buoyancy parameter ( $N$ ), mixed convection parameter ( $\lambda$ ), Magnetic parameter ( $M$ ) and Suction parameter ( $S$ ). Observed temperature profile for Magnetic parameter ( $M$ ), mixed convection parameter ( $\lambda$ ), Thermophoresis parameter ( $Nt$ ), Biot number ( $Bi$ ), Heat source/sink Parameter ( $Hg$ ), Thermal relaxation parameter ( $\delta_T$ ), Prandtl Number ( $Pr$ ), Eckert number ( $Ec$ ), Radiation parameter ( $R$ ). Examined concentration profile for Activation Energy (A.E.), temperature difference ( $\delta$ ), Thermophoresis parameter ( $Nt$ ), Magnetic parameter ( $M$ ), chemical reaction rate constant ( $\sigma^*$ ), parameter of Brownian motion ( $Nb$ ), Solute relaxation parameter ( $\delta_C$ ), and Schmidt Number ( $Sc$ ). Additionally, for a range of values, the local Sherwood number, skin friction coefficient, and local Nusselt number were obtained.

**Keywords.** Activation energy, Zero normal flux, Casson Nano fluid, Exponential stretching sheet, Cattaneo-Christov heat flux

**Mathematics Subject Classification (2020).** 76M55, 76A05, 76S05, 65L06, 76M20, 65L10, 80A32, 80A21

## 1. Introduction

Due to its many applications in various industrial manufacturing processes and engineering like wire drawing, extrusion of plastic, hot rolling and rubber sheets, glass blowing, fibre spinning, metallic plates' condensation process, aerodynamics, and many others, the study of mass and heat transmission of laminar boundary layer flow across a stretching sheet has quickly advanced. Stretching and concurrent heating or cooling have a significant impact on the end goods' quality during such procedures. Modern metallurgical and medicinal fields are very interested in the magnetohydrodynamic (MHD) flow of a fluid that is electrically conducting. Examples of these domains include the coating of metals, magnetohydrodynamic (MHD) power production systems, cooling of nuclear reactors, wound healing, and the use of MRI to diagnose diseases and perform surgical procedures. Due to its broad range of technological applications, substantial research has been done on boundary layer flow that is brought on by an exponentially stretched sheet. For instance, the final result depends on changes in temperature distribution and stretching velocity when copper wires are annealed and tinned. In such operations, the quality of the final outputs is significantly influenced by both the concurrent heating or cooling and the kinematics of stretching. Choi originated the term "nanofluid" to describe dispersions of nanoparticles in common fluids including propylene glycol, water, and ethylene glycol. Choi demonstrated that the thermal conductivity of traditional heat transfer liquids could be improved up to almost two times by the addition of a tiny quantity (<1% by volume) of nanoparticles. A fluid that detracts from Newton's viscosity law is referred to as non-Newtonian. It is necessary to study non-Newtonian fluid ideas in order to fully understand nature of common fluids. Researchers are interested in fluids that are non-Newtonian in nature, because of their complexity and large range of scientific and industrial applications. Non-Newtonian fluids comprise, for instance, tangent hyperbolic fluids, Casson fluid, Maxwell, Power-law fluids, Williamson fluids, and Jeffrey fluids. Such fluids contain the non-Newtonian Casson fluid, which displays yield stress. The influences of heat generation and absorption on mass and heat transmission have been the subject of extensive experimental and theoretical research in recent years. Applications for heat source/sink include heat source or sink modification in polymer manufacturing, cooling electronic equipment, cooling/heating of plastic items, etc. On the other hand, because thermal radiation has such an extensive range of applications in physics, engineering, and space technology, it has a considerable impact on the mass and heat transfer of different fluids over a stretching surface. For instance, in the industry of manufacturing polymers, thermal radiation effects may be a significant factor in managing heat transfer. Some significant uses of radiative heat transfer consist of high-temperature plasmas, nuclear power plants, cooling of nuclear reactors, MHD accelerators, liquid metal fluids, spacecraft and satellites.

Engineers, scientists, and researchers were driven to study "Non-Newtonian fluid boundary layer flow with heat and mass transmission over stretched surfaces" because of the wide-ranging applications. Svante Arrhenius developed the term "Arrhenius activation" in 1889. The minimum level energy necessary for a chemical system with potential reactants to initiate a chemical reaction is simulated. *A.E.*'s effects on "convective heat and mass transmission in boundary layer region" were assessed by Bestman [5]. Since then, numerous studies have

taken place to check how  $A.E.$  affects mass and heat transmission in boundary layer flow of the fluid. The impact of  $A.E.$  on mass and heat transmission in unstable flow of fluid under several geometries was studied by Anurada and Sashikala [3], Dhlamini *et al.* [7], and Hamid *et al.* [11]. Sarwe *et al.* [22] looked at the Casson hybrid nanofluid flow across a plate moving vertically under the impact of magnetic field and ( $A.E.$ ) activation energy with convective boundary conditions. Atif *et al.* [4] studied the magnetohydrodynamic Casson nanofluid and activation energy under the influence of exponential, temperature-dependent, and variable viscosity, thermal conductivity on a stretched surface.

With the help of his heat conduction model, Fourier (in 1822) took the decision to look into the various practical situations in which heat transmission occurs. The parabolic heat equation is produced as a result of this law, which demonstrates how the initial disturbances has an immediate impact on the system under investigation. The result is a clear denial of the notion of heat conduction. In order to address this issue, Fourier significantly altered the law of heat conduction (Jabeen *et al.* [15]). Cattaneo, with the addition of thermal relaxation time in 1948 has given a new heat conduction law that produced a hyperbolic equation allowing energy to be transferred via waves. Under various boundary conditions, many researchers examined activation energy employing Cattaneo-Christov heat flux (see Eswaramoorthi *et al.* [8], Ijaz *et al.* [13], Muhammad *et al.* [17]). The concept of heat flux given by Cattaneo-Christov was examined by Ali and Sandeep [2], Prasad *et al.* [19], Ramana *et al.* [20] for a range of fluids in various settings. Using the Keller box methodology, Malik *et al.* [16] studied about MHD flow of Casson fluid with the model of Cattaneo-Christov heat flux and variable viscosity. Bilal *et al.* [6] carried out a numerical analysis of 2D viscoelastic fluid driven by surface stretched exponentially with magnetic effects. Aligned magnetic field, heterogeneous-homogeneous chemical reaction, Cattaneo-Christov heat flux, of Casson fluid flow across a stretching surface were all investigated by Reddy and Suneetha [21].

Gangiah *et al.* [10] inspected the effects of a heat source and thermal radiation on the MHD, mixed convection flow of Casson nanofluid across a sheet stretched exponentially. Ittedi *et al.* [14] examined the influences of chemical reaction, magnetic field, and heat source/sink on heat transmission of a nanofluid on a stretching sheet at the boundary by taking thermal slip, velocity slip, and concentration slip into account. The effects of a viscous dissipation, as well as, heat source on a Jeffrey fluid flow through a vertical plate were examined by Muzara *et al.* [18] in their study. Gangiah *et al.* [9] examined how viscosity dissipation along with chemical reaction affects flow of non-Newtonian nanofluid flow across an exponentially extending sheet. Abualnaja [1] employed the Homotopy perturbation method to examine the flow of MHD Williamson fluid on an exponentially stretched sheet with convective boundary condition.

The primary goal of the current study is to look at the effects of the activation energy ( $A.E.$ ) of a mixed convective, a Magnetohydrodynamic (MHD) Casson fluid flow with “zero normal flux of nanoparticles over a sheet” stretched exponentially in the presence of heat source/sink and radiation parameters, along with the convective boundary condition and Cattaneo-Christov heat flow. We took into account a “zero normal flux of nanoparticles” defined in boundary conditions, to exclude gravitational effects at the sheet’s surface. The results of the nondimensional velocity,

concentration, and temperature tests were illustrated with graphs thoroughly and presented quantitatively in tables for the Sherwood, Nusselt number, and skin friction coefficient.

## 2. Mathematical Formulation

Consider a steady, two-dimensional (2D), laminar, mixed convection boundary layer flow over a sheet stretched exponentially along with thermal radiation, heat source/sink and Cattaneo-Christov heat flux. A variable magnetic field  $B(x)$  taken normal to the surface. Applied suction and convective heat condition at the sheet's surface. On the basis of application of two opposite and equal forces at a time along the x-axis, it is assumed that the flow is produced by stretching the sheet with a strong force until its velocity is exponential in nature. The y-axis is perpendicular to the x-axis and x-axis is assumed to be the stretching surface in the fluid flow's direction. The flow is contained to  $y > 0$  and concurs with the plane  $y = 0$ . The sheet is then stretched while the origin is held fixed, with velocity  $U_w$  and  $T_w$  as the surface temperature. It is assumed that nanoparticle mass flux at the wall is zero.

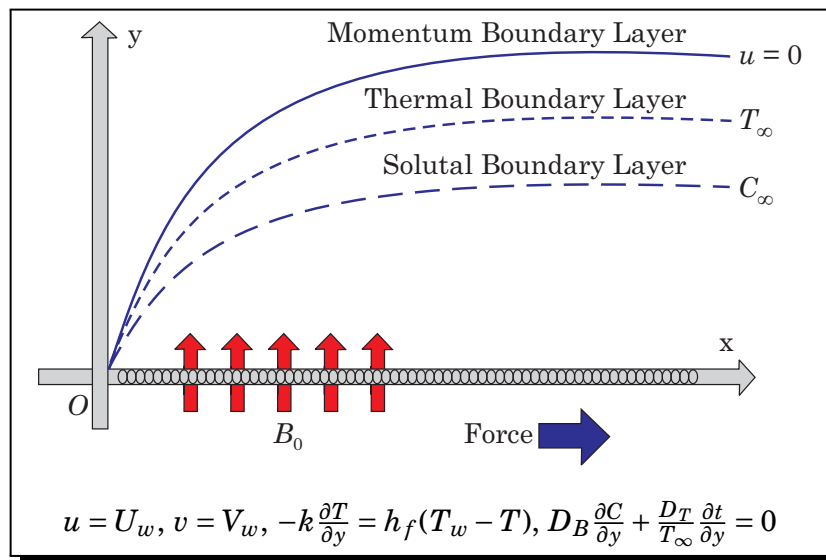


**Figure 1.** Fluid flow physical model

The sheet is subjected to an evolving magnetic field  $B = B_0 e^{x/2L}$  where  $B_0$  is the magnetic field's initial intensity. All of these factors lead to the following governing equations for this flow's continuity, momentum, energy, and concentration (Bilal *et al.* [6], Gangaiah *et al.* [10], Younus and Lakshmi [23]):

Continuity equation is given by

$$\frac{\partial v}{\partial y} + \frac{\partial u}{\partial x} = 0. \tag{1}$$

Momentum equation is given by

$$u \frac{\partial u}{\partial x} + v \frac{\partial u}{\partial y} = \nu \left( 1 + \frac{1}{\beta} \right) \frac{\partial^2 u}{\partial y^2} + g\beta_t(T - T_\infty) + g\beta_c(C - C_\infty) - \frac{\sigma B_0^2}{\rho_f} u. \tag{2}$$

The equation of energy is

$$\begin{aligned}
 u \frac{\partial T}{\partial x} + v \frac{\partial T}{\partial y} + \lambda_T \omega_T \\
 = \frac{k}{\rho c_p} \frac{\partial^2 T}{\partial y^2} + \frac{\mu}{\rho c_p} \left( \frac{\partial u}{\partial y} \right)^2 - \frac{1}{\rho c_p} \frac{\partial q_r}{\partial y} + \tau \left[ D_B \frac{\partial C}{\partial y} \frac{\partial T}{\partial y} + \frac{D_T}{T_\infty} \left( \frac{\partial T}{\partial y} \right)^2 \right] + \frac{Q}{\rho c_p} (T - T_\infty).
 \end{aligned} \tag{3}$$

The equation of concentration is

$$u \frac{\partial C}{\partial x} + v \frac{\partial C}{\partial y} + \lambda_C \omega_C = \frac{D_T}{T_\infty} \frac{\partial^2 T}{\partial y^2} + D_B \frac{\partial^2 C}{\partial y^2} - k_r^2 (C - C_\infty) \left( \frac{T}{T_\infty} \right)^n e^{-\left( \frac{E_a}{kT} \right)}, \tag{4}$$

where

$$\omega_T = v \frac{\partial v}{\partial y} \frac{\partial T}{\partial y} + u \frac{\partial u}{\partial x} \frac{\partial T}{\partial x} + u^2 \frac{\partial^2 T}{\partial x^2} + v^2 \frac{\partial^2 T}{\partial y^2} + 2uv \frac{\partial^2 T}{\partial x \partial y} + v \frac{\partial u}{\partial y} \frac{\partial T}{\partial x} + u \frac{\partial v}{\partial x} \frac{\partial T}{\partial y} \tag{5}$$

and

$$\omega_C = u \frac{\partial u}{\partial x} \frac{\partial C}{\partial x} + v \frac{\partial v}{\partial y} \frac{\partial C}{\partial y} + u^2 \frac{\partial^2 C}{\partial x^2} + v^2 \frac{\partial^2 C}{\partial y^2} + 2uv \frac{\partial^2 C}{\partial x \partial y} + u \frac{\partial v}{\partial x} \frac{\partial C}{\partial y} + v \frac{\partial u}{\partial y} \frac{\partial C}{\partial x}. \tag{6}$$

The problem’s boundary conditions are as follows (Gangaiah *et al.* [10]):

$$u = U_w, v = V_w, -k \frac{\partial T}{\partial y} = h_f (T_w - T) \text{ and } D_B \frac{\partial C}{\partial y} + \frac{D_T}{T_\infty} \frac{\partial T}{\partial y} = 0, \text{ at } y = 0 \tag{7}$$

and  $u \rightarrow 0, T \rightarrow T_\infty, C \rightarrow C_\infty$  as  $y \rightarrow \infty$ .

From the above equations, we have  $u$  and  $v$  as velocity components respectively along  $X$  and  $Y$  axes,  $\mu$  stands for viscosity coefficient, density of the fluid as  $\rho$ ,  $g$ ,  $\beta$  stand for the gravitational acceleration and Casson fluid parameter respectively,  $\beta_c$  and  $\beta_t$  stands for coefficients of the concentration and thermal expansion respectively,  $C$  represents concentration and  $T$  represents temperature of fluid,  $T_\infty, C_\infty$  as ambient fluid temperature and fluid concentration respectively,  $\sigma$  as the fluid’s electrical conductivity,  $k$  represents the thermal conductivity,  $Q = Q_0 e^{x/2L}$  is “the temperature dependent volumetric rate of heat source when  $Q > 0$  and heat sink when  $Q < 0$ ,  $Q_0$  is a constant”, and  $c_p$  stand for fluid’s specific heat under constant pressure,  $q_r$  stands for the radiative heat flux, kinematic viscosity is expressed as  $\nu = \frac{\mu}{\rho}$ ,  $\tau = \frac{(\rho c)_p}{(\rho c)_f}$  represents “the ratio of nanoparticle heat capacity to base fluid heat capacity”,  $D_B$  represents Brownian diffusion and  $D_T$  represents thermal diffusion coefficients respectively, and  $K_c = k_0 e^{\frac{x}{L}}$  is the chemical conversion rate of irreversible reaction of first order. In the boundary conditions,  $U_w = U_0 e^{\frac{x}{L}}$  is elongating velocity, where  $U_0$  is the position velocity, and the characteristic length denoted by  $L$ ,  $V_w = -v_0 e^{\frac{x}{2L}}$  is special type velocity on the wall. Here  $v_0$  is the starting suction strength,  $V_w < 0$  stands for the flow rate of blowing, and  $V_w > 0$  stands for flow rate of suction, the convective heat transfer coefficient is denoted by  $h_f$ , whereas  $T_w$  stands for the sheet’s convective fluid temperature,  $k_r$  is designated as the response rate parameter,  $E_a$  is (A.E.) the activation energy and ‘ $n$ ’ represents fitted rate constant.

On simplification of radiative heat flux

$$q_r = \frac{-4\alpha^1}{3k^1} \frac{\partial T^4}{\partial y}, \tag{8}$$

$$T^4 \cong T_\infty^3 (4T - 3T_\infty). \tag{9}$$

On using (9) in (8), we get

$$q_r = \frac{-16\alpha^1}{3k^1} T_\infty^3 \frac{\partial T}{\partial y}. \tag{10}$$

### 3. Solution Methodology

By the below similarity transformations, we can convert the system to *O.D.E* from a system of *P.D.E*.

$$\left. \begin{aligned} \eta(x, y) &= \sqrt{\frac{U_0}{2\nu L}} e^{\frac{x}{2L}} y, \quad \psi(x, y) = \sqrt{2U_0\nu L} e^{\frac{x}{2L}} f(\eta), \\ T &= T_\infty + (T_w - T_\infty)\theta(\eta), \quad C = C_\infty + (C_\infty) \cdot \phi(\eta) \end{aligned} \right\}, \tag{11}$$

where  $\eta$  as the similarity variable,  $f(\eta)$  as stream function,  $\theta(\eta)$  as dimensionless temperature function and  $\phi(\eta)$  as concentration function, and  $\psi(x, y)$  is the stream function.

Continuity equation is getting satisfied with the selection of  $\psi(x, y)$  such that

$$u = \frac{\partial \psi}{\partial y}, \quad v = -\frac{\partial \psi}{\partial x}.$$

Therefore,

$$u = U_0 e^{\frac{x}{L}} f'(\eta), \quad v = -\sqrt{\frac{\nu U_0}{2L}} e^{\frac{x}{2L}} (\eta f'(\eta) + f(\eta)). \tag{12}$$

By substituting the aforementioned conversions (11)-(12) in equations (2)-(4), we get a system of *O.D.E*

$$\left(1 + \frac{1}{\beta}\right) f'''(\eta) + f(\eta)f''(\eta) - 2[f'(\eta)]^2 + \lambda[\theta(\eta) + N\phi(\eta)] - Mf'(\eta) = 0 \tag{13}$$

$$\begin{aligned} \frac{1}{Pr} \left[1 + \frac{4R}{3} - Pr \delta_T [f(\eta)]^2\right] \theta''(\eta) + \theta'(\eta) \cdot f(\eta) + Ec [f''(\eta)]^2 \\ + Nb \theta'(\eta) \phi'(\eta) + Nt [\theta'(\eta)]^2 + Hg \cdot \theta(\eta) = 0, \end{aligned} \tag{14}$$

$$\begin{aligned} \phi''(\eta) - \phi'(\eta) Le Pr \delta_C [f(\eta)]^2 + Le Pr f(\eta) \phi'(\eta) + \frac{Nt}{Nb} \theta''(\eta) \\ + Le Pr \delta_C f(\eta) \cdot \phi'(\eta) \cdot \phi'(\eta) - \sigma^* Le Pr e^{-\left(\frac{E}{1+\theta\delta}\right)} (1 + \theta\delta)^n \phi(\eta) = 0. \end{aligned} \tag{15}$$

Therefore, we get from (7) dimensionless boundary conditions as

$$\left. \begin{aligned} f(\eta) = S, \quad f'(\eta) = 1, \quad \theta'(\eta) = Bi[\theta(\eta) - 1], \quad Nb \cdot \phi'(\eta) + Nt \cdot \theta'(\eta) = 0 \text{ at } \eta = 0, \\ \text{and } f'(\eta) \rightarrow 0, \quad \theta(\eta) \rightarrow 0, \quad \phi(\eta) \rightarrow 0 \text{ as } \eta \rightarrow \infty \end{aligned} \right\}, \tag{16}$$

where  $\beta = \mu_B \frac{\sqrt{2\pi c}}{P_y}$  is the Casson fluid parameter, Mixed convection parameter is  $\lambda = \frac{2Lg\beta_t(T_w - T_\infty)}{U_w^2}$ ,  $N = \frac{\beta_c(C_w - C_\infty)}{\beta_t(T_w - T_\infty)}$ , the buoyancy parameter. Prandtl number is  $Pr = \frac{\mu}{k} c_p = \frac{\nu}{\alpha}$ ,  $M = \frac{2L\sigma B_0^2}{U_0\rho}$  stands for parameter of magnetic field,  $R = \frac{4\alpha^1}{kk^1} T_\infty^3$  is the radiation parameter in which  $\alpha^1$  denotes Stefan-Boltzmann Constant,  $k^1$  stands for coefficient of absorption,  $Ec = \frac{U_w^2}{c_p(T_w - T_\infty)}$  representing Eckert number,  $\delta_T = \frac{U_w}{2L} \lambda_T$  is for Thermal relaxation parameter, Brownian motion parameter is  $Nb = \frac{\tau D_B(C_w - C_\infty)}{\nu}$ ,  $Q = Q_0 e^{x/2L}$  is “the temperature dependent volumetric rate of heat source when  $Q > 0$  and heat sink when  $Q < 0$ ,  $Q_0$  is a constant”,  $Le = \frac{\alpha}{D_B}$

is the Lewis number,  $Nt = \frac{\tau D T(T_w - T_\infty)}{v T_\infty}$  for the parameter of thermophoresis,  $K_I = \frac{2Lk_0}{U_0}$  stands for chemical reaction parameter,  $S = \nu_0 \sqrt{\frac{2L}{vU_0}} > 0$  is the parameter of suction, Biot number,  $Bi = \frac{h_f}{k} \sqrt{\frac{2L\nu}{U_w}}$ ,  $\sigma^* = \frac{K_I}{K_c} k_r^2$  is the “chemical reaction rate constant”,  $\delta_C = \frac{U_w}{2L} \lambda_C$  represents solute relaxation parameter  $E = \frac{E_a}{kT_\infty}$  is the Activation Energy (A.E.) and  $\delta = \frac{(T_w - T_\infty)}{T_\infty}$ , the temperature difference. Coefficient of skin friction  $C_{f_x} = \frac{\tau_w}{\rho U_w^2}$ , Local Nusselt number  $N_{u_x} = \frac{xq_w}{k(T_w - T_\infty)}$ , Local Sherwood number  $S_{h_x} = \frac{xq_m}{D_B(C_w - C_\infty)}$  (Gangaiah *et al.* [10]),

$$(Re_x)^{\frac{1}{2}} C_{f_x} = \left(1 + \frac{1}{\beta}\right) f''(0), \tag{17}$$

$$(Re_x)^{-\frac{1}{2}} N_{u_x} = -\left(1 + \frac{4R}{3}\right) \theta'(0), \tag{18}$$

$$(Re_x)^{-\frac{1}{2}} S_{h_x} = -\phi'(0), \tag{19}$$

were  $Re_x = \frac{xU_w}{\nu}$  is local Reynold’s number.

### 4. Numerical Procedure

The equation set from (13) to (15) and also the boundary conditions (16) are difficult to solve analytically. Using the 4th order Runge-Kutta (RK) method and the shooting methodology described by Younus and Lakshmi [23], these equations were numerically solved. This approach is still one of the most exact and successful ways of solving boundary layer flows. It is vital to make a choice of the suitable finite numbers for the boundary conditions for  $\theta(\eta)$  and  $\theta'(\eta)$  at  $\eta = 0$ . To find  $\eta_\infty$ , we begin with a first guess value for a certain set of physical factors to obtain the values of  $f''(0)$ ,  $\theta'(0)$  and  $\phi'(0)$ . We first reduce the aforementioned differential equations (D.E.) using the variables shown below:

$$f = f_1, f' = f_2, f'' = f_3, \theta = f_4, \theta' = f_5, \phi = f_6, \phi' = f_7. \tag{20}$$

Equations (13) through (15) are changed by using the variables from (20), and the result is the order one differential equation system that is shown below (Bilal *et al.* [6], Gangaiah *et al.* [10]):

$$f_1' = f_2 = f_2, \tag{21}$$

$$f_2^1 = f_3 = f_3, \tag{22}$$

$$f_3^1 = f_3' = \frac{[2(f_2)^2 - f_1 f_3 + M f_2 - \lambda(f_4 + N f_6)]}{[1 + \frac{1}{\beta}]}, \tag{23}$$

$$f_4^1 = f_5 = f_5, \tag{24}$$

$$f_5^1 = f_5' = \frac{Pr}{(Pr \delta_T (f_1)^2 - 1 - \frac{4R}{3})} [f_1 f_5 + Ec(f_3)^2 + \delta_T f_1 f_2 f_5 + Nb f_5 f_7 + Nt(f_5)^2 + Hg f_4], \tag{25}$$

$$f_6^1 = f_7 = f_7, \tag{26}$$

$$f_7^1 = f_7' = \left[ \frac{Nt}{Nb} \frac{Pr}{(Pr \delta_T (f_1)^2 - 1 - \frac{4R}{3})} [f_1 f_5 + Ec(f_3)^2 + \delta_T f_1 f_2 f_5 + Nb f_5 f_7] \right]$$

$$\begin{aligned}
 & + Nt(f_5)^2 + Hg f_4] - Le Pr \sigma^* (1 + \delta\theta)^n e^{-\left(\frac{E}{1+\delta\theta}\right)} \phi(\eta) + Le \cdot Pr f_1 f_7 + Le Pr \delta_C f_1 f_2 f_7 \Big] \\
 & \cdot \left[ \frac{1}{(Le Pr \delta_C (f_1)^2 - 1)} \right]. \tag{27}
 \end{aligned}$$

The reformed boundary conditions are

$$\left. \begin{aligned}
 & f_1(\eta) = S, f_2(\eta) = 1, f_5(\eta) = Bi[f_4(\eta) - 1], Nb \cdot f_7(\eta) + Nt \cdot f_5(\eta) = 0 \text{ at } \eta = 0, \\
 & \text{and } f_2(\eta) \rightarrow 0, f_4(\eta) \rightarrow 0, f_6(\eta) \rightarrow 0 \text{ as } \eta \rightarrow \infty
 \end{aligned} \right\} \tag{28}$$

For the set of equations (21) through (27) and the boundary conditions (28) to be solved, a value of  $\theta(0) = f_4(0)$ ,  $\theta'(0) = f_5(0)$ , is necessary but such a value is not provided. The appropriate guess values are selected for  $f(\eta)$ ,  $\theta(\eta)$  and  $\phi(\eta)$  in order to attain the values of  $\theta(0)$  in the MATLAB technique utilising the Runge-Kutta (RK) process with the operation of shooting, adopting step size as  $\Delta\eta = 0.01$ . In order to make  $\theta'(0) = 1$ . We used the parameters  $\eta_{max} = 3$ ,  $\theta(0) = 2$ , and we compared the created values of  $-\theta'(0)$  to the results that previously existed. Until the outcomes are converging and fall within such a tolerance [10, 23] of  $10^{-4}$ . this procedure is repeated.

### 5. Discussion on Findings

Using the MATLAB programme with the Runge-Kutta (RK) Method, investigated the behaviour of the temperature, nanoparticle volume fraction profile, and velocity profile with governing parameters. Figures 2-23 and Tables 1-4 present the findings. Except for a few occasions, we utilised  $N = Ec = \lambda = 0.3$ ,  $Pr = 6.9$ ,  $M = \beta = Bi = Nt = Nb = 0.5$ ,  $S = 0.2$ ,  $\sigma^* = 0.5$ ,  $\delta = 0.3$ ,  $E = 1$ ,  $n = 0.5$ ,  $Hg = 0.2$ ,  $\delta_T = \delta_C = 0.1$ ,  $Sc = 8$ , and  $R = 0.6$  for graph plotting during the analysis.

We physically discussed the graphical results of the problem to underline the results. The velocity boundary layer is reduced when the Casson fluid parameter  $\beta$  increases, as shown in Figure 2. The rise in  $\beta$  causes the fluid’s plastic dynamic viscosity to increase, which lowers the fluid’s velocity profiles by raising the fluid’s internal resistance. The fluid’s velocity increases as the mixed convection factor  $\lambda$  is raised, as shown in Figure 3. An advantageous pressure gradient is produced and fluid flow is accelerated as a result of the rise in  $\lambda$ , which also generates a large increase in thermal buoyancy. This causes the velocity boundary layer to thicken as  $\lambda$  increases, while the temperature profile shows the opposite pattern in Figure 11. Figure 5 shows how the buoyancy parameter  $N$  affects profile of velocity. A similar explanation may be given for the behaviour of the buoyancy parameter, which causes the fluid’s velocity to increase as  $N$  increases. The impact of  $S$ , the suction parameter on boundary layer profiles of velocity is seen in Figure 6. The fluid is forced to migrate closer to the sheet because of increased suction, which raises resistance and diminishes profiles of velocity. Magnetic parameters’ effects on the velocity curve, temperature curve, and concentration curve are shown in Figures 4, 10, and 20. It shows that as the magnetic parameter enhances, the velocity profile decreases. Some useful energy is converted into heat due to the Lorentz force, produced by the magnetic field’s existence and resists fluid motion. Because of this, as  $M$  is raised, the temperature and concentration rise but the flow velocity falls. Figure 7 shows how the radiation parameter  $R$

affects the thermal boundary layer. As  $R$  rises, thermal boundary layer thickness develops along with the temperature, increasing the flow of radiative heat. Figure 8 illustrates how the Prandtl number affects the temperature curve. Here, we observed that when the  $Pr$  value increased, the temperature profile decreased. Thermal diffusivity decreases as  $Pr$  increases. This implies that the ability to transport energy has reduced and the thermal barrier layer has become thinner. According to Figure 13, the temperature profile rises with increasing Eckert number. The Eckert number is indeed the ratio between difference in boundary layer enthalpy and kinetic energy. Since an increase in  $Ec$  leads to an increase in K.E., from motion, the fluid will extract energy and convert it into thermal energy. Due to this the fluid becomes heated. How the Brownian motion parameter  $Nb$  impacts the concentration profile is depicted in Figure 19. The thickness of the concentration boundary layer thins because  $Nb$  boosts fluid diffusion. Figures 9 and 18 show how the thermophoresis parameter  $Nt$  affects temperature and concentration profiles. It exhibits that as  $Nt$  grows, thermophoresis force rises, leading nanoparticles to move to a cold surface from a hot one. This causes the temperature to rise and the concentration boundary layer to thicken. As  $Hg$ , the heat source/sink parameter increases, Figure 12 shows that the thickness of thermal boundary layer also increases. In fact, the temperature field of the fluid's thermal barrier layer increases as  $Hg$  increases. Figure 15 shows the effect of  $Bi$ , the Biot number, on temperature profiles. The ratio of "thermal conductivity to heat transfer rate" is denoted by the dimensionless metric known as  $Bi$ . Better temperature profiles are the result of  $Bi$ , which increases the heat flux. The temperature profile's impact on  $\delta_T$  thermal relaxation parameter is shown in Figure 14. It is evident that the fluid's temperature decreases as thermal relaxation parameter rise. A possible physical explanation for this might be that the material's particles require more amount of time to transfer energy to their nearby neighbours when the thermal relaxation increases. Therefore, a rise in thermal relaxation parameter will accompany a fall in the temperature profile. Figure 16 shows how volume fraction profile of nanoparticles are impacted by the "chemical reaction rate constant"  $\sigma^*$ . In a result, as  $\sigma^*$ , increases, the fluid's concentration will drop. As the values of  $\sigma^*$  increases, the Arrhenius expression rises as well, ultimately harming the chemical reaction. The Schmidt number  $Sc$  has an impact on the volume fraction profile of nanoparticles, as shown in Figure 17. It illustrates how, when  $Sc$  inclines, the mass diffusivity and, subsequently, thickness of boundary layer of concentration decrease. Figure 21 illustrates how the volume fraction profile of nanoparticles are impacted by activation energy  $E$ . Thermophoresis parameter increases are correlated with temperature increases, which are correlated with increases in  $A.E.$ , which are correlated with increases in chemical reaction rates and boundary layer concentration. Due to this, concentration boundary layer thickness grows as  $E$  rises. Temperature variations have an impact on the volume fraction profile of nanoparticles, as seen in Figure 23. The boundary layer thickness of the concentration decreases as the temperature difference widens. From Figure 22 we can see that as the solute relaxation parameter increases, nanoparticle volume fraction decreases.

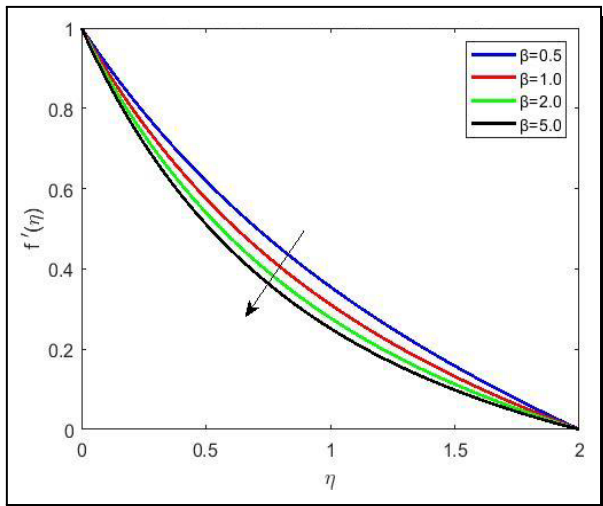


Figure 2. Variations in velocity profile for  $\beta$

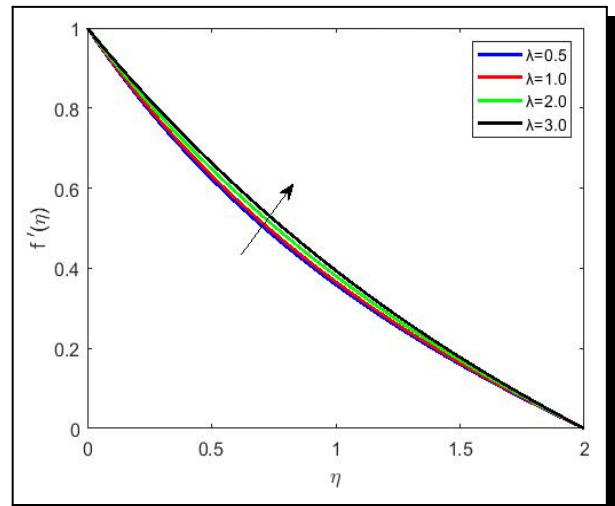


Figure 3. Variations in velocity profile for  $\lambda$

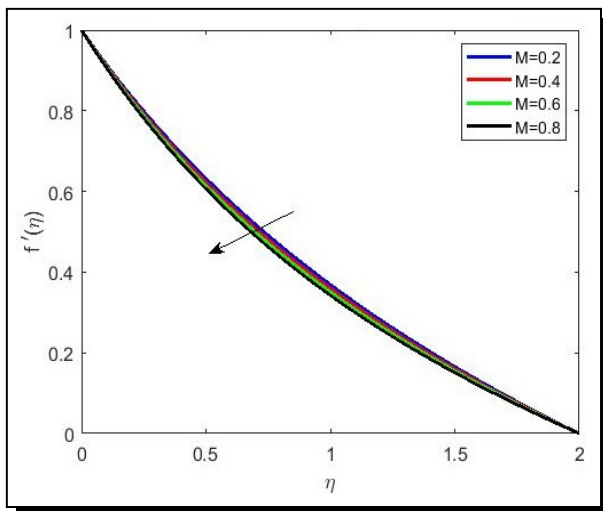


Figure 4. Variations in velocity profile for  $M$

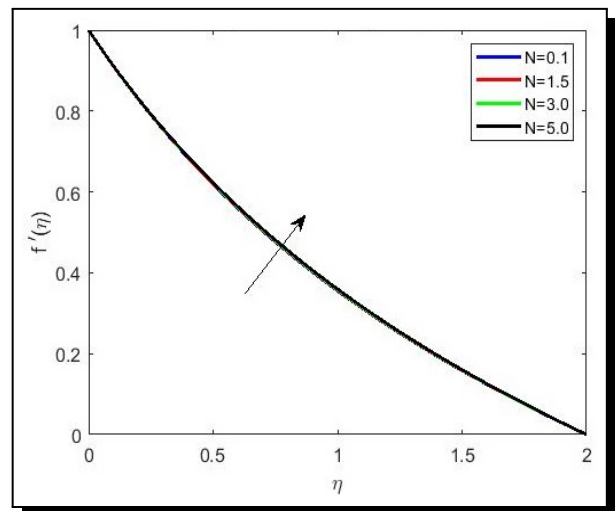


Figure 5. Variations in velocity profile for  $N$

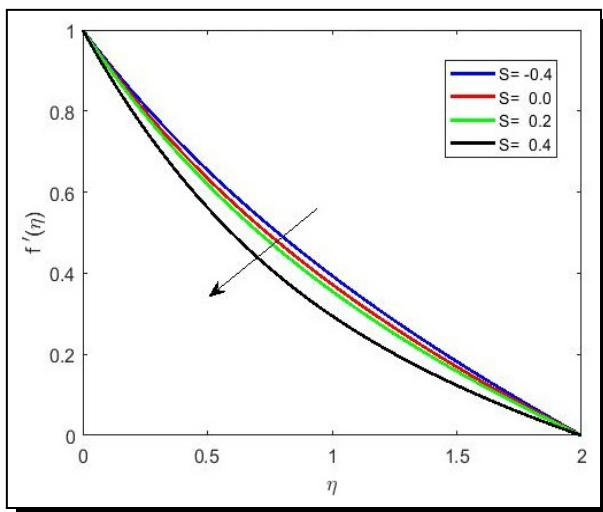


Figure 6. Variations in velocity profile for  $S$

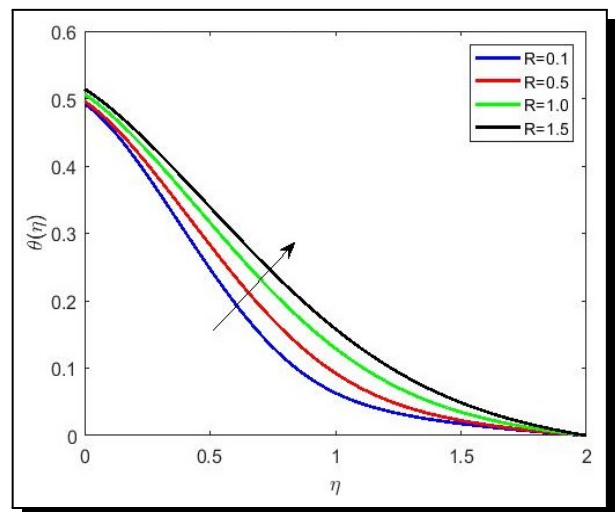
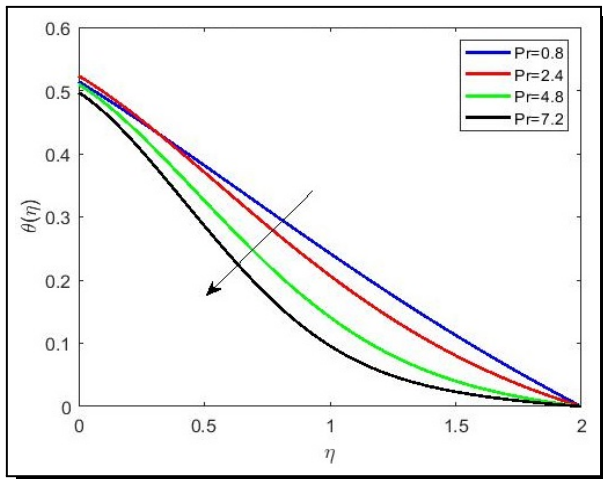
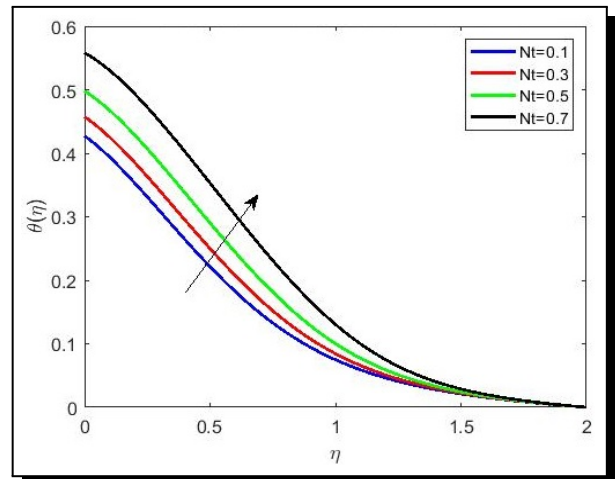


Figure 7. Variation in temperature profile for  $R$



**Figure 8.** Variations in temperature profile for  $Pr$



**Figure 9.** Variations in temperature profile for  $Nt$

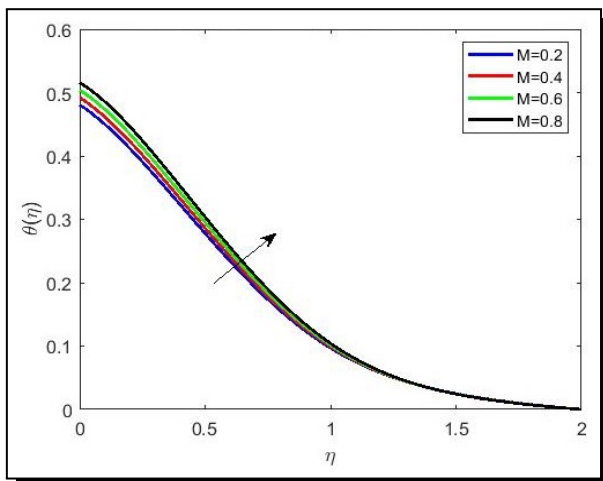


**Figure 10.** Variations in temperature profile for  $M$

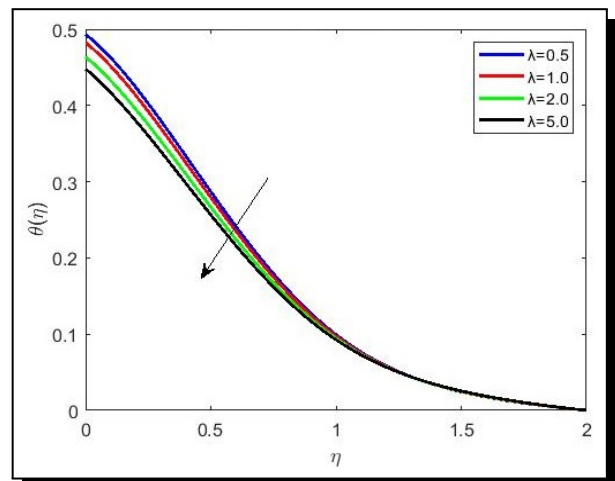


**Figure 11.** Variation in temperature profile for  $\lambda$

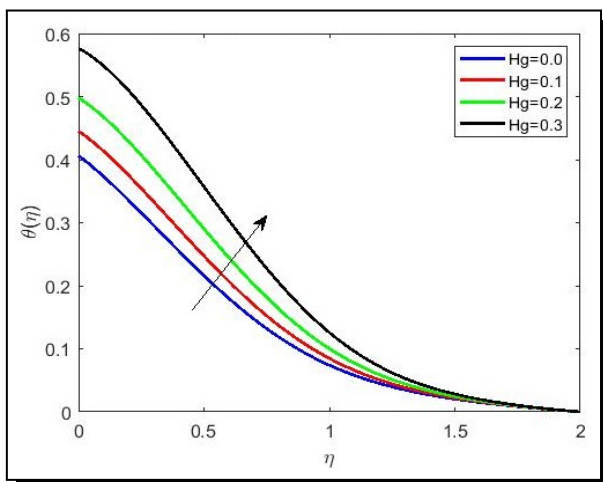


**Figure 12.** Variation in temperature profile for  $Hg$

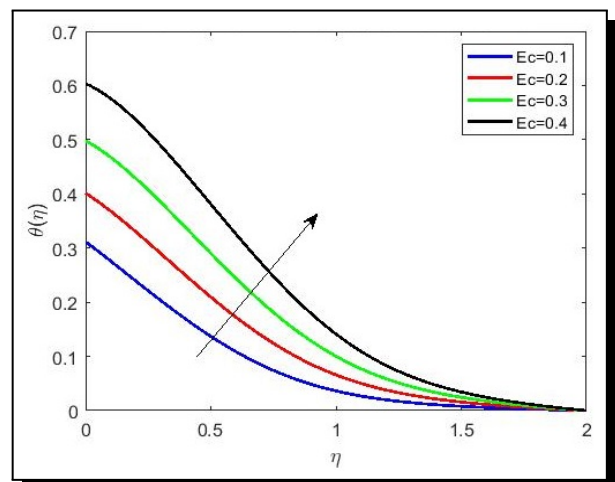


**Figure 13.** Variation in temperature profile for  $Ec$

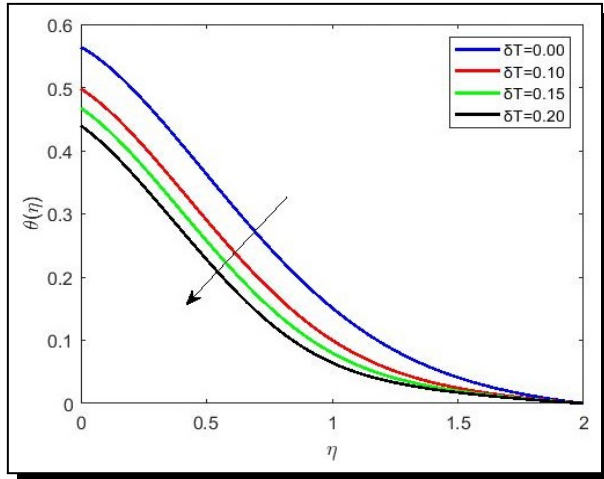


Figure 14. Variation in temperature profile for  $\delta T$

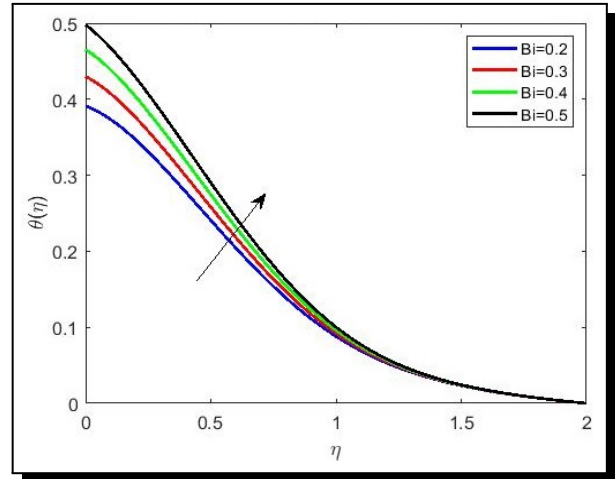


Figure 15. Variation in temperature profile for  $Bi$

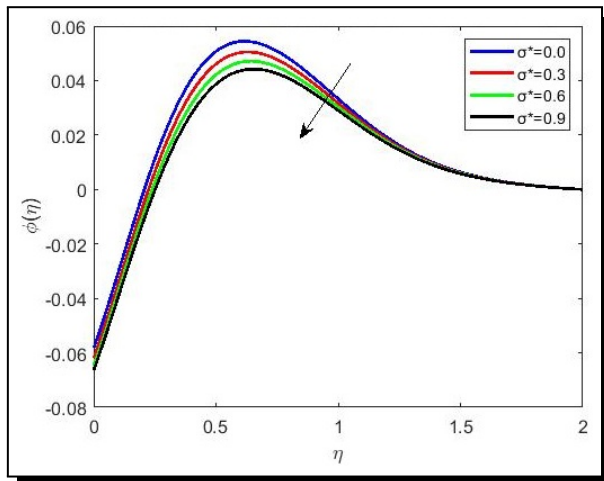


Figure 16. Variation in nanoparticle volume fraction for  $\sigma^*$

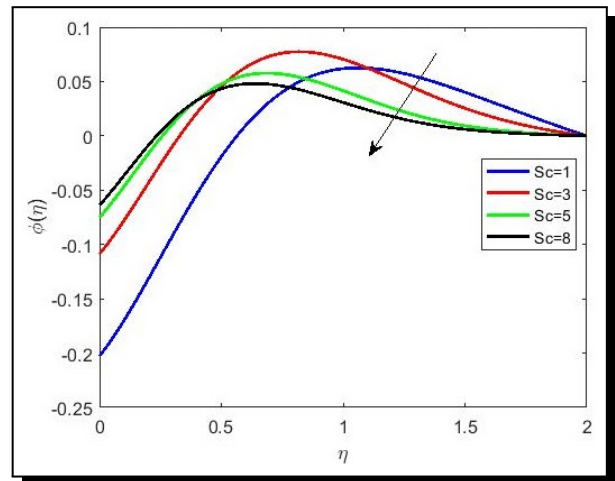


Figure 17. Variations in nanoparticle volume fraction for  $Sc$

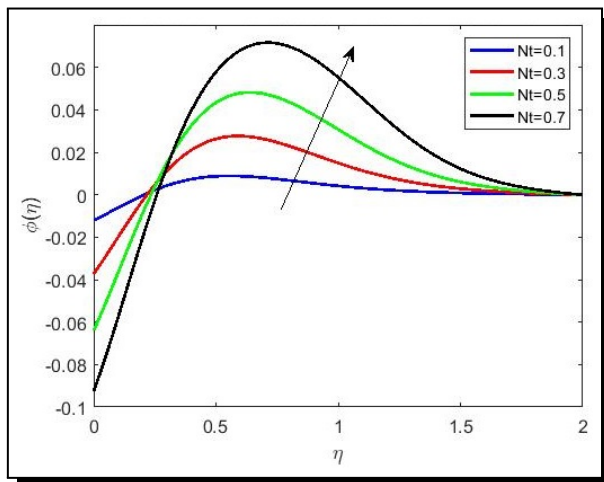


Figure 18. Variation in nanoparticle volume fraction for  $Nt$

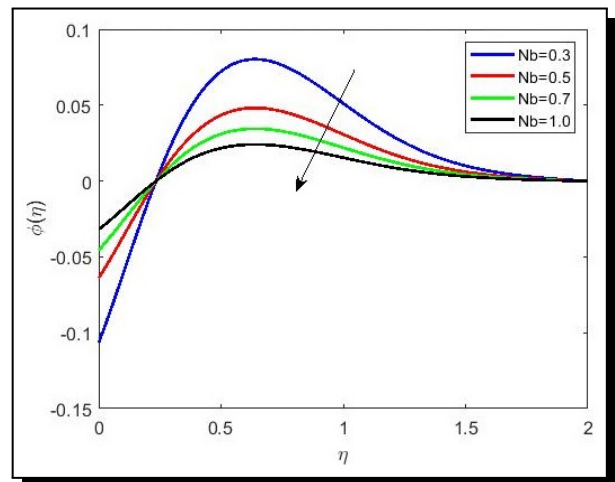


Figure 19. Variation in nanoparticle volume fraction for  $Nb$

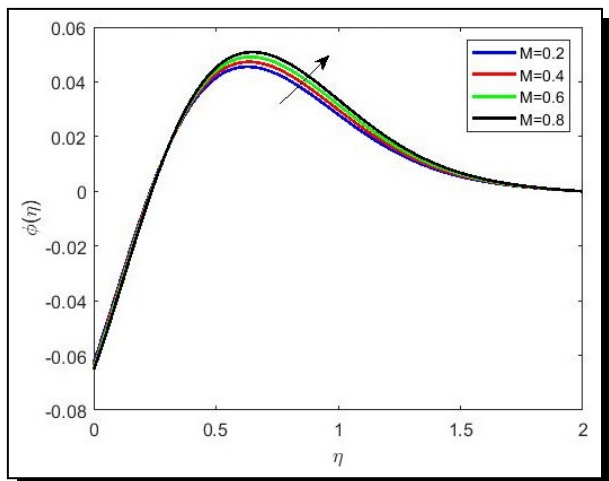


Figure 20. Variations in nanoparticle volume fraction for  $M$

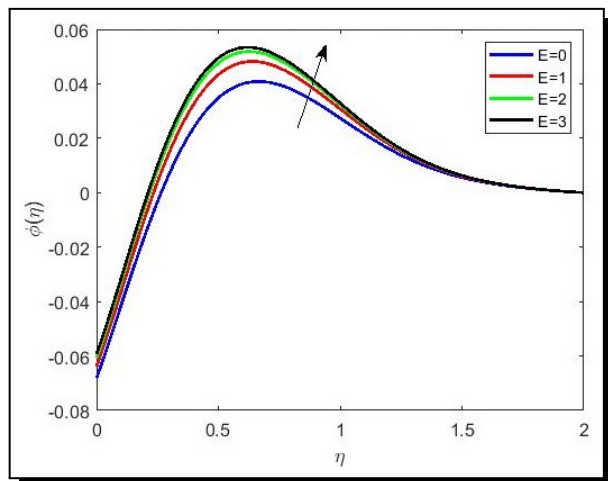


Figure 21. Variations in nanoparticle volume fraction for  $E$

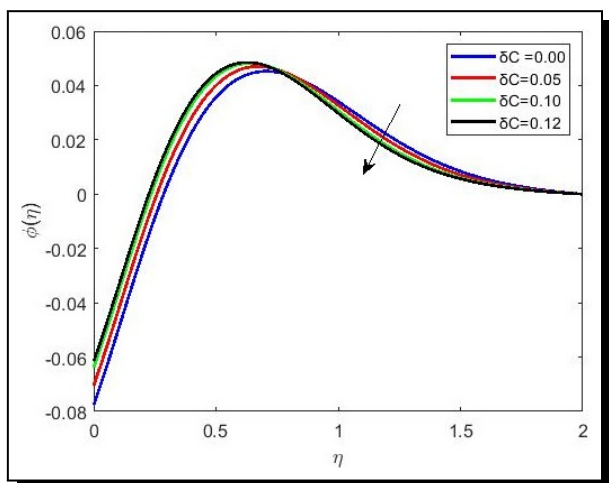


Figure 22. Variations in nanoparticle volume fraction for  $\delta C$

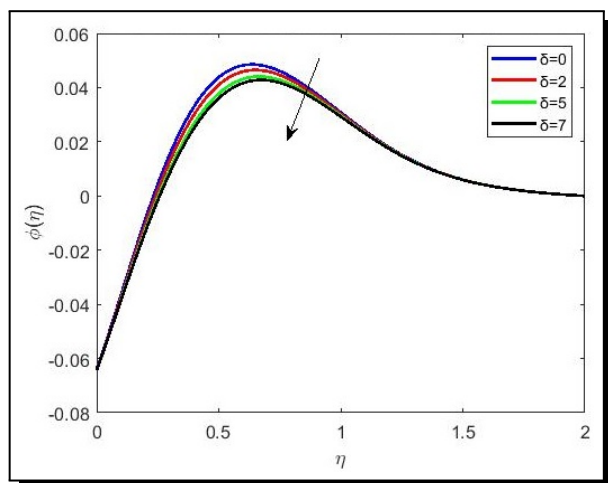


Figure 23. Variations in nanoparticle volume fraction for  $\delta$

Table 1. Comparison of  $[-\theta'(0)]$  for various  $\beta$ ,  $Nt$  and  $Nb$  values, when  $Hg = M = R = 0$ ,  $S = 0$ ,  $Bi = 0.2$ ,  $\lambda = N = 0.3$ ,  $Sc = 0.7$

$\beta$	$Nt$	$Nb$	Hayat <i>et al.</i> [12]	Gangiah <i>et al.</i> [10]	Present values
0.5	0.2	0.2	0.15271	0.15281	0.152923
0.7			0.15204	0.15197	0.152430
0.9			0.15150	0.15136	0.152073
0.2	0.2	0.2	0.15271	0.15281	0.152923
	0.4		0.15195	0.15267	0.152784
	0.6		0.15106	0.15106	0.152643
0.5	0.2	0.2	0.15271	0.15281	0.152923
		0.4	0.15186	0.15280	0.152926
		0.6	0.15100	0.15279	0.152927

On Comparison of  $[-(2Re_x)^{\frac{1}{2}}C_{f_x}]$ , the skin friction coefficient to the results of Hayat *et al.* [12], Gangaiah *et al.* [10] in Table 1 for different  $\beta$ ,  $Nt$  and  $Nb$ , values, outcomes are found to be in strong agreement with previous.

From Table 2 we got the information that local skin friction coefficient value enhances with  $\beta$  and  $\lambda$  and declines with  $S$  and  $M$ . From Table 3 we have that local Nusselt number falls when  $Nt$ ,  $\beta$ ,  $Ec$ ,  $Hg$  and  $M$  values increase, while the opposite is true for  $Pr$  and  $R$ . Table 4, has shown that local Sherwood number grew with increases in  $Sc$ ,  $\sigma^*$ ,  $\delta_C$ , and  $\delta$  and fall with increases in  $E$ ,  $Pr$  and  $Nt$ .

**Table 2.** Skin friction Coefficient for different parameters

S. No.	$M$	$\beta$	$S$	$\lambda$	$(Re_x)^{\frac{1}{2}}C_{f_x}$
1	0	0.5			-2.566605
2		1			-1.991566
3		2			-1.679888
4	0.5	0.5			-2.802953
5		1			-2.200563
6		2			-1.867564
7	1	0.5			-3.027007
8		1			-2.395609
9		2			-2.040251
10	0			0.5	-2.526286
11				1	-2.428497
12				1.5	-2.334483
13	0.5			0.5	-2.760926
14				1	-2.659475
15				1.5	-2.562514
16	1			0.5	-2.983087
17				1	-2.877589
18				1.5	-2.777369
19			0		-2.659516
20			0.1		-2.735779
21			0.2		-2.802953

**Table 3.** Nusselt number for different parameter values

S. No.	$M$	$\beta$	$Pr$	$Nt$	$R$	$Ec$	$Hg$	$(Re_x)^{\frac{1}{2}}N_{u_x}$
1	0.3							0.538083
2	0.6							0.530700
3	0.9							0.522835
4		0.5						0.533214
5		1						0.502862
6		2						0.468363
7			1.7					0.468756
8			5					0.528943
9			7.5					0.542033
10				0				0.633352
11				0.5				0.533214
12				1				0.288647
13					0.2			0.402663
14					0.4			0.468855
15					0.8			0.596092
16						0.2		0.564838
17						0.4		0.469944
18						0.6		0.309053
19							-0.2	0.615436
20							-0.1	0.583348
21							0.1	0.578790
22							0.2	0.533214

**Table 4.** Sherwood Number for different parameter values

S. No.	$P$	$Nt$	$\sigma^*$	$Sc$	$E$	$\delta$	$\delta_C$	$(Re_x)^{-\frac{1}{2}} Sh_x$
1	1.7							-0.213408
2	5							-0.257542
3	7							-0.277010
4		0						-0.000000
5		0.5						-0.272269
6		1						-0.287884
7			0.5	1.7				-0.326219
8				5				-0.297656
9				8.5				-0.270152
10			1	1.7				-0.322428
11				5				-0.292128
12				8.5				-0.265435
13			1.5	1.7				-0.318640
14				5				-0.286300
15				8.5				-0.260411
16					0			-0.265637
17					0.5			-0.269789
18					1			-0.272269
19					1.5			-0.273735
20						0		-0.273044
21						0.3		-0.272269
22						0.6		-0.271516
23							0	-0.281806
24							0.05	-0.280709
25							0.1	-0.279566

## 6. Conclusions

Final observations of the present work are the following.

The fluid velocity profile increases with a rise in the parameter of mixed convection, the buoyancy parameter, and it decreases with a rise in Casson fluid parameter, the magnetic field

parameter, and the suction parameter. While thickness of thermal boundary layer declines with increasing values of the Prandtl number, mixed convection parameter, thermal relaxation parameter, it increases with rising of the radiation parameter, thermophoresis, magnetic field parameter, parameter of heat source/sink, Eckert number, and Biot number. With increment in value of chemical reaction rate constant, temperature difference, Solute relaxation parameter, Brownian motion parameter, and Schmidt number, the profile of nanoparticle volume fraction decreases; conversely, it increases as  $A.E.$ , Schmidt number, thermophoresis, and magnetic field parameters all increase. The skin friction coefficient rises due to the Casson fluid, and mixed convection parameter, whereas it falls due to suction parameter, and magnetic field parameter. The local Nusselt number grows with the Prandtl number and radiation parameter and falls with Casson fluid, the thermophoresis, magnetic field, heat source or sink parameters and Eckert number. Local Sherwood number rises along with “chemical reaction rate constant”, temperature difference, Schmidt number, and solute relaxation parameter, while it falls along with the thermophoresis parameter, Prandtl number, and activation energy ( $A.E.$ ).

### Competing Interests

The authors declare that they have no competing interests.

### Authors' Contributions

All the authors contributed significantly in writing this article. The authors read and approved the final manuscript.

## References

- [1] K. M. Abualnaja, Homotopy perturbation method for MHD non-Newtonian Williamson fluid over exponentially stretching sheet with viscous dissipation and convective boundary condition, *International Journal of Modern Physics C* **30**(11) (2019), 1950088, DOI: 10.1142/S0129183119500888.
- [2] M. E. Ali and N. Sandeep, Cattaneo-Christov model for radiative heat transfer of magnetohydrodynamic Casson-ferrofluid: A numerical study, *Results in Physics* **7** (2017), 21 – 30, DOI: 10.1016/j.rinp.2016.11.055.
- [3] S. Anuradha and K. Sasikala, MHD free convective flow of a nanofluid over a permeable shrinking sheet with binary chemical reaction and activation energy, *International Journal of Engineering Science Invention* **7**(1) (2018), 22 – 30.
- [4] S. M. Atif, S. Shah and A. Kamran, Effect of MHD on Casson fluid with Arrhenius activation energy and variable properties, *Scientia Iranica* **29**(6) (2022), 3570 – 3581, DOI: 10.24200/sci.2021.57873.5452.
- [5] A. R. Bestman, Natural convection boundary layer with suction and mass transfer in a porous medium, *International Journal of Energy Research* **14**(4) (1990), 389 – 396, DOI: 10.1002/er.4440140403.
- [6] S. Bilal, M. Y. Malik, M. Awais, Khalil-ur-Rehman, A. Hussain and I. Khan, Numerical investigation on 2D viscoelastic fluid due to exponentially stretching surface with magnetic effects: An application of non-Fourier flux theory, *Neural Computing and Applications* **30**(9) (2018), 2749 – 2758, DOI: 10.1007/s00521-016-2832-4.

- [7] M. Dhlamini, P. K. Kameswaran, P. Sibanda, S. Motsa and H. Mondal, Activation energy and binary chemical reaction effects in mixed convective nanofluid flow with convective boundary conditions, *Journal of Computational Design and Engineering* **6**(2) (2019), 149 – 158, DOI: 10.1016/j.jcde.2018.07.002.
- [8] S. Eswaramoorthi, N. Alessa, M. Sangeethavaanee, S. Kayikci and N. Namgyel, Mixed convection and thermally radiative flow of MHD Williamson nanofluid with Arrhenius activation energy and Cattaneo-Christov heat-mass flux, *Journal of Mathematics* **2021** (2021), 2490524, DOI: 10.1155/2021/2490524.
- [9] T. Gangaiah, N. Saidulu and A. V. Lakshmi, Magnetohydrodynamic flow of nanofluid over an exponentially stretching sheet in presence of viscous dissipation and chemical reaction, *Journal of Nanofluids* **7**(3) (2018), 439 – 448, DOI: 10.1166/jon.2018.1465.
- [10] T. Gangaiah, N. Saidulu and A. V. Lakshmi, The influence of thermal radiation on mixed convection MHD flow of a casson nanofluid over an exponentially stretching sheet, *International Journal of Nanoscience and Nanotechnology* **15**(2) (2019), 83 – 98.
- [11] A. Hamid, Hashim and M. Khan, Impacts of binary chemical reaction with activation energy on unsteady flow of magneto-Williamson nanofluid, *Journal of Molecular Liquids* **262** (2018), 435 – 442, DOI: 10.1016/j.molliq.2018.04.095.
- [12] T. Hayat, M. B. Ashraf, S. A. Shehzad and A. Alsaedi, Mixed convection flow of Casson nanofluid over a stretching sheet with convectively heated chemical reaction and heat source/sink, *Journal of Applied Fluid Mechanics* **8**(4) (2015), 803 – 813, DOI: 10.18869/acadpub.jafm.67.223.22995.
- [13] M. Ijaz, M. S. Alqarni, F. Salah and M. Y. Malik, Numerical simulation of Joule heating and Arrhenius activation energy for nonlinear radiative flow of Casson nanofluid with Cattaneo–Christov heat flux model, *Physica Scripta* **95**(2) (2020), 025401, DOI: 10.1088/1402-4896/ab41ac.
- [14] S. Ittedi, D. Ramya and S. Joga, MHD heat transfer of nanofluids over a stretching sheet with slip effects and chemical reaction, *International Journal of Latest Engineering Research and Applications* **2**(8) (2017), 10 – 20.
- [15] S. Jabeen, T. Hayat, S. Qayyum and A. Alsaedi, Significance of activation energy in stratified flow of tangent hyperbolic fluid, *International Journal of Numerical Methods for Heat & Fluid Flow* **29**(8) (2019), 2932 – 2947, DOI: 10.1108/HFF-12-2018-0795.
- [16] M. Y. Malik, M. Khan, T. Salahuddin and I. Khan, Variable viscosity and MHD flow in Casson fluid with Cattaneo–Christov heat flux model: Using Keller box method, *Engineering Science and Technology, an International Journal* **19**(4) (2016), 1985 – 1992, DOI: 10.1016/j.jestch.2016.06.008.
- [17] T. Muhammad, A. Alsaedi, S. A. Shehzad and T. Hayat, A revised model for Darcy-Forchheimer flow of Maxwell nanofluid subject to convective boundary condition, *Chinese Journal of Physics* **55**(3) (2017), 963 – 976, DOI: 10.1016/j.cjph.2017.03.006.
- [18] H. Muzara and S. Shateyi, MHD laminar boundary layer flow of a Jeffrey fluid past a vertical plate influenced by viscous dissipation and a heat source/sink, *Mathematics* **9**(16) (2021), 1896, DOI: 10.3390/math9161896.
- [19] K. V. Prasad, H. Vaidya, K. Vajravelu and V. Ramanjini, Analytical study of Cattaneo-Christov heat flux model for Williamson-nanofluid flow over a Slender elastic sheet with variable thickness, *Journal of Nanofluids* **7**(3) (2018), 583 – 594, DOI: 10.1166/jon.2018.1475.
- [20] K. V. Ramana, K. Gangadhar, T. Kannan, and A. J. Chamkha, Cattaneo–Christov heat flux theory on transverse MHD Oldroyd-B liquid over nonlinear stretched flow, *Journal of Thermal Analysis and Calorimetry* **147**(3) (2022), 2749 – 2759, DOI: 10.1007/s10973-021-10568-x.

- [21] P. B. A. Reddy and S. Suneetha, Impact of Cattaneo-Christov heat flux in the Casson fluid flow over a stretching surface with aligned magnetic field and homogeneous – Heterogeneous chemical reaction, *Frontiers in Heat and Mass Transfer* **10** (2018), Article number 7, 9 pages, DOI: 10.5098/hmt.10.7.
- [22] D. U. Sarwe, B. Shanker, R. Mishra, R. S. V. Kumar and M. N. R. Shekar, Simultaneous impact of magnetic and Arrhenius activation energy on the flow of Casson hybrid nanofluid over a vertically moving plate, *International Journal of Thermofluid Science and Technology* **8**(2) (2021), Paper number 080202, DOI: 10.36963/ijtst.2021080202.
- [23] M. Younus and A. V. Lakshmi, Numerical investigation of activation energy of radiative magnetohydrodynamic Williamson nanofluid flow, *Heat Transfer* **51**(7) (2022), 6197 – 6222, DOI: 10.1002/htj.22588.

